Journal of Sound and Vibration 326 (2009) 837–851

Contents lists available at ScienceDirect

Journal of Sound and Vibration

journal homepage: www.elsevier.com/locate/jsvi

In-plane free vibration of functionally graded circular arches with temperature-dependent properties under thermal environment

P. Malekzadeh [a,b], M.M. Atashi [a], G. Karami [c,*]

[a] Department of Mechanical Engineering, Persian Gulf University, Bushehr 75168, Iran
[b] Center of Excellence for Computational Mechanics, Shiraz University, Shiraz, Iran
[c] Department of Mechanical Engineering and Applied Mechanics, North Dakota State University, Fargo, ND 58108-6050, USA

ARTICLE INFO

Article history:
Received 10 November 2008
Received in revised form
11 April 2009
Accepted 13 May 2009
Handling Editor: C.L. Morfey
Available online 13 June 2009

ABSTRACT

Analysis of in-plane free vibration of functionally graded (FG) thin-to-moderately thick deep circular arches in thermal environments is presented based on first-order shear deformation theory (FSDT). The material properties are assumed to be temperature-dependent and graded in the thickness direction. Hamilton's principle is employed to derive the equations of motion and the related boundary conditions including the effects of initial thermal stresses. The temperature is assumed to be uniform through the arch surface and varied through the thickness. The initial thermal stresses are obtained by solving the thermoelastic equilibrium equations. The differential quadrature method (DQM) as an efficient numerical tool is adopted to solve the thermoelastic equilibrium equations and the equations of motion. The numerical solutions are validated by comparing to the solutions of the limited cases for isotropic arches, as well as by examining the solutions convergence behavior. Parametric studies are also conducted to study the effects of the temperature rise, boundary conditions and the material graded index on the frequency of the FG arches. Also, the impact of geometrical parameters such as the thickness-to-mean radius ratio and the opening angle are examined.

1. Introduction

In recent years a new class of materials known as functionally graded materials (FGMs) with a continuous change in their material domain, particularly along the thickness direction has emerged. Structural elements made of FGMs, such as; circular arches have found widespread applications in space vehicles, aircrafts, automobiles, nuclear power plants and many other industries. These elements are often exposed to dynamic thermal environments with large temperature changes which induce thermoelastic stresses that affect the behavior of the system. Hence, vibration characteristic of functionally graded (FG) structures under high-temperature environment is of interest for engineering design.

There have been some investigations on the in-plane free vibration analysis of composite arches mostly limited to laminated arches with orthotropic layers [1–6]. Also free vibration analyses of FG straight beams with and without thermal effects have come under consideration [7–13]; a brief discussion is in order here. Aydogdu and Taskin [7] used different higher-order shear deformation theories and classical beam theory to investigate the free vibration of simply supported FG beams using Navier's method. The natural frequencies and mode shapes of a simply supported FG beam were also examined by Li [8] based on the first-order shear deformation theory (FSDT). Sina et al. [9] introduced an analytical

* Corresponding author. Tel.: +1701 231 5859; fax: +1701 231 8913.
E-mail address: G.Karami@ndsu.nodak.edu (G. Karami).

0022-460X/$ - see front matter © 2009 Elsevier Ltd. All rights reserved.
doi:10.1016/j.jsv.2009.05.016

approach based on FSDT beam theory to examine the free vibration of FG beams under various boundary conditions. Yang and Chen [10] presented a theoretical investigation for free vibration and elastic buckling of FG beams containing open edge cracks using the Bernoulli–Euler beam theory. Ying et al. [11] presented an analytical solution for bending and free vibration of functionally graded simply supported beams resting on elastic foundation based on two-dimensional theory of elasticity. The problem was solved using the state space method in conjunction with trigonometric series. Bhangale and Ganesan [12] studied the buckling and vibration behaviors of clamped FG sandwich beams having constrained viscoelastic layer subjected to thermal environment using finite element method. Pradhan and Murmu [13] studied thermomechanical vibration of FG beams and FG sandwich beams resting on elastic foundation using modified differential quadrature method (MDQM). Xiang and Yang [14] studied free and forced vibration of laminated FG beams of variable thickness under thermally induced initial stresses within the framework of Timoshenko beam theory and used the differential quadrature method (DQM) for the analysis.

In this paper, free vibration behavior of FG circular arches in thermal environments and with temperature-dependent material properties is studied. In order to include the transverse shear deformation and rotary inertia effects on natural frequencies, the first-order shear deformation theory is to be employed. The material properties are thus assumed temperature-dependent and graded in the thickness direction. The Hamilton's principle is employed to derive the equations of motion and the related boundary conditions. The initial thermal stresses are obtained by solving the thermoelastic equilibrium equations. DQM as an efficient numerical tool [15–19] is employed to solve the governing differential equations. The convergence behavior and accuracy of the presented method are investigated through different examples. The influences of uniform and non-uniform temperature rise, boundary conditions, dependence of material properties on temperature, material property graded index and geometrical parameters on the in-plane vibration frequencies of FG arches will be studied.

2. Theoretical formulation

Consider a thick FG circular arch as shown in Fig. 1. A polar coordinate system (r,θ) is used to label the material points of the arch in the unstressed reference configuration. The displacement components of an arbitrary material point (r,θ) of the arch are denoted as $\bar{u}$ and $\bar{v}$ in r- and θ-directions, respectively.

2.1. Temperature dependent FGMs relations

The material properties of the arch are assumed to vary continuously through the thickness, i.e. in the r-direction. In this study, without the loss of generality of the formulations, the material properties are assumed to vary according to power law distribution in terms of volume fractions of the constituents through the thickness. The material composition continuously varies such that the outer surface of the arch ($r = R_o$) is ceramic-rich whereas the inner surface of the arch ($r = R_i$) is metal-rich. Based on the power law distribution, a typical effective material property 'P' of the FG arch is obtained as

$$P(r,T) = P_m(T) + [P_c(T) - P_m(T)]\left(\frac{r - R_i}{h}\right)^p, \tag{1}$$

where the subscripts m and c refer to the metal and ceramic constituents, respectively, p the power law index or the material property graded index, h the thickness of the arch and $T\,[=T(r)]$ the temperature at an arbitrary material point of the arch.

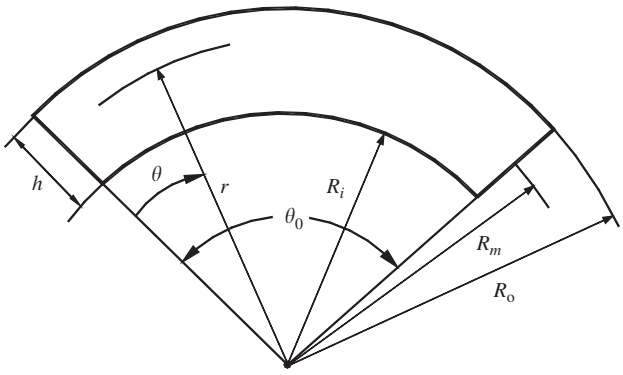

Fig. 1. Geometry and coordinate system of the FGM circular arch.

For the FG arch constituents, i.e. ceramic and metal, the material properties are temperature-dependent and a typical property 'Q' may be expressed as a function of temperature as [20,21]

$$Q(T) = Q_0(1 + Q_1T + Q_2T^2). \tag{2}$$

The coefficients Q_i $(i = 0, 1, 2)$ are unique to the constituent materials.

2.2. Thermal analysis

It is assumed that the arch is stress free at the temperature T_0. If the arch operates in a thermal environment, non-uniform temperature rise or mechanical constraints at its edges cause deformation and consequently create some stresses in it. These stresses affect the vibration characteristic of the arch. In order to evaluate these thermal stresses, the temperature distribution in the arch should be obtained firstly. Here, it is assumed that the temperature rise varies only across the section of arch and no heat generation source exists within the arch. Hence, the temperature distribution along the thickness direction can be obtained by solving the following steady-state one-dimensional heat transfer equations through the thickness of the arch:

$$\mathrm{K}(r)\frac{\mathrm{d}^2T}{\mathrm{d}r^2} + \frac{\mathrm{dK}(r)}{\mathrm{d}r}\frac{\mathrm{d}T}{\mathrm{d}r} = 0, \tag{3}$$

where K is the thermal conductivity of the arch. Different thermal boundary conditions can be considered at the inner and the outer surfaces of the arch. One of the thermal boundary conditions usually considers prescribed temperature at the upper and lower surfaces of these structural elements. Hence, for the brevity purpose and without loss of generality, here these type of the boundary conditions are considered, which for an arch problem become

$$T = T_m \ \text{ at } \ r = R_i \quad \text{and} \quad T = T_c \ \text{ at } \ r = R_o. \tag{4}$$

The solution to Eq. (3) subjected to the boundary conditions (4) can be obtained by means of polynomial series solutions. The result is

$$T(r) = T_m + \frac{\Delta T}{C}\left[\left(\frac{r-R_i}{h}\right) - \frac{\mathrm{K}_{cm}}{(p+1)\mathrm{K}_m}\left(\frac{r-R_i}{h}\right)^{p+1} + \frac{\mathrm{K}_{cm}^2}{(2p+1)\mathrm{K}_m^2}\left(\frac{r-R_i}{h}\right)^{2p+1} - \frac{\mathrm{K}_{cm}^3}{(3p+1)\mathrm{K}_m^3}\left(\frac{r-R_i}{h}\right)^{3p+1} + \frac{\mathrm{K}_{cm}^4}{(4p+1)\mathrm{K}_m^4}\left(\frac{r-R_i}{h}\right)^{4p+1} - \frac{\mathrm{K}_{cm}^5}{(5p+1)\mathrm{K}_m^5}\left(\frac{r-R_i}{h}\right)^{5p+1}\right], \tag{5}$$

where $\Delta T = T_c - T_m$, $\mathrm{K}_{cm} = \mathrm{K}_c - \mathrm{K}_m$ and

$$C = 1 - \frac{\mathrm{K}_{cm}}{(p+1)\mathrm{K}_m} + \frac{\mathrm{K}_{cm}^2}{(2p+1)\mathrm{K}_m^2} - \frac{\mathrm{K}_{cm}^3}{(3p+1)\mathrm{K}_m^3} + \frac{\mathrm{K}_{cm}^4}{(4p+1)\mathrm{K}_m^4} - \frac{\mathrm{K}_{cm}^5}{(5p+1)\mathrm{K}_m^5}.$$

2.3. Vibration analysis

To study the free vibration characteristic of a FG arch in thermal environment, the displacement components of an arbitrary material point (r, θ) are perturbed around its equilibrium position. Hence, the total displacement components measured from the arch undeformed configurations become $\bar{u}_0(r,\theta) + \bar{u}(r,\theta,t)$ and $\bar{v}_0(r,\theta) + \bar{v}(r,\theta,t)$ along the r- and θ-directions, respectively. Hereafter, a subscript '0' is used to represent the variables of deformation field and stress components in the equilibrium state of the arch in thermal environment. The thermoelastic equilibrium equations and the free vibration equations of motion together with the related boundary conditions can be obtained in a systematic manner by using the Hamilton's principle, which has the following form:

$$\int_{t_1}^{t_2} (\delta K - \delta U)\,\mathrm{d}t = 0, \tag{6}$$

where K and U are the kinetic and the potential energy of the arch and t_1 and t_2 are the beginning and the end of motion time, respectively. The variational form of the arch potential energy can be stated as

$$\delta U = \int_0^{\theta_0}\int_{R_i}^{R_o} [(\sigma_{0\theta\theta} + \sigma_{\theta\theta})\delta(\varepsilon_{0\theta\theta} + \varepsilon_{\theta\theta}) + (\sigma_{0r\theta} + \sigma_{r\theta})\delta(\gamma_{0r\theta} + \gamma_{r\theta})]br\,\mathrm{d}r\,\mathrm{d}\theta, \tag{7}$$

where $\varepsilon_{0\theta\theta}$, $\gamma_{0r\theta}$ and $\sigma_{0\theta\theta}$, $\sigma_{0r\theta}$ are the normal and the shear components of the strain tensor and stress tensor at equilibrium state, $\varepsilon_{\theta\theta}$, $\gamma_{r\theta}$ and $\sigma_{\theta\theta}$, $\sigma_{r\theta}$ are the normal and the shear components of the strain tensor and stress tensor due to vibration, also, θ_0, R_i, R_o and b are the opening angle, inner radius, outer radius and width of the arch, respectively.

Since in this study only small amplitude free vibration is considered, the nonlinear terms are to be neglected. Hence, the strain–displacement relations of the thermoelastic equilibrium state become

$$\varepsilon_{0\theta\theta}=\frac{1}{r}\left(\frac{\partial\bar{v}_0}{\partial\theta}+\bar{u}_0\right),\quad \gamma_{0r\theta}=\frac{1}{r}\left(\frac{\partial\bar{u}_0}{\partial\theta}-\bar{v}_0\right)+\frac{\partial\bar{v}_0}{\partial r}. \tag{8}$$

However, to include the effects of the initial stresses due to thermal environment in the equations of motion, the nonlinear terms in the strain–displacement relations of vibration should be considered

$$\varepsilon_{\theta\theta}=\varepsilon^{L}_{\theta\theta}+\varepsilon^{NL}_{\theta\theta}=\frac{1}{r}\left(\frac{\partial\bar{v}}{\partial\theta}+\bar{u}\right)+\frac{1}{2r^2}\left(\frac{\partial\bar{u}}{\partial\theta}-\bar{v}\right)^2+\frac{1}{2r^2}\left(\frac{\partial\bar{v}}{\partial\theta}+\bar{u}\right)^2,$$

$$\gamma_{r\theta}=\gamma^{L}_{\theta\theta}+\gamma^{NL}_{\theta\theta}=\frac{1}{r}\left(\frac{\partial\bar{u}}{\partial\theta}-\bar{v}\right)+\frac{\partial\bar{v}}{\partial r}+\frac{1}{r}\left(\frac{\partial\bar{u}}{\partial\theta}-\bar{v}\right)\frac{\partial\bar{u}}{\partial r}+\frac{1}{r}\left(\frac{\partial\bar{v}}{\partial\theta}+\bar{u}\right)\frac{\partial\bar{v}}{\partial r}, \tag{9}$$

where the superscripts '*L*' and '*NL*' stand for the linear and nonlinear terms of the strain components.

Employing the small amplitude vibration assumption, the stress–strain relations become

$$\sigma_{0\theta\theta}=E(r,T)[\varepsilon_{0\theta\theta}(r,\theta)-\alpha(r,T)\Delta T(r)],\quad \sigma_{0r\theta}=\kappa G(r,T)\gamma_{0r\theta}(r,\theta),$$

$$\sigma_{\theta\theta}=E(r,T)\varepsilon^{L}_{\theta\theta}(r,\theta),\quad \sigma_{r\theta}=\kappa G(r,T)\gamma^{L}_{r\theta}(r,\theta), \tag{10}$$

where $E(r,T)$ is the Young's modulus, $\alpha(r,T)$ the thermal expansion coefficient of the arch, $T(r)$ the temperature at an arbitrary material point of the arch, $\Delta T(r)=T(r)-T_0$ the temperature rise,

$$G(r,T)\left[=\frac{0.5E(r,T)}{1+v(r,T)}\right]$$

the shear rigidity and κ the shear correction factor.

The variational form of the arch kinetic energy is obtained from the following equation:

$$\delta K=\int_0^{\theta_0}\int_{R_i}^{R_o}\rho\left(\frac{\partial\bar{u}}{\partial t}\frac{\partial\delta\bar{u}}{\partial t}+\frac{\partial\bar{v}}{\partial t}\frac{\partial\delta\bar{v}}{\partial t}\right)b r\,\mathrm{d}r\,\mathrm{d}\theta, \tag{11}$$

where $\rho[=\rho(r,T)]$ is the mass density of the FG arch.

Based on the FSDT, the displacement components at an arbitrary material point (r,θ) of the arch can be expressed as

$$\bar{u}_0(r,\theta)=u_0(\theta),\quad \bar{v}_0(r,\theta)=v_0(\theta)+x\varphi_0(\theta),\quad \bar{u}(r,\theta,t)=u(\theta,t),\quad \bar{v}(r,\theta,t)=v(\theta,t)+x\varphi(\theta,t), \tag{12}$$

where $\varphi(\theta)$ is the bending rotation of the cross section of the arch, also, $x=r-R_m$ and R_m the mean radius of the arch.

Inserting Eqs. (7)–(12) into Eq. (6) and performing the integration by parts with respect to spatial coordinate variables θ and time t, one obtains the thermoelastic equilibrium equations and the equations of motion together with the related boundary conditions as follows:

Thermoelastic equilibrium equations:

$$\delta u_0:\ A_s\frac{\mathrm{d}^2u_0}{\mathrm{d}\theta^2}-A_nu_0-(A_s+A_n)\frac{\mathrm{d}v_0}{\mathrm{d}\theta}+(A_sR_m-B_n)\frac{\mathrm{d}\varphi_0}{\mathrm{d}\theta}=-N_T, \tag{13}$$

$$\delta v_0:\ (A_s+A_n)\frac{\mathrm{d}u_0}{\mathrm{d}\theta}+A_n\frac{\mathrm{d}^2v_0}{\mathrm{d}\theta^2}-A_sv_0+B_n\frac{\mathrm{d}^2\varphi_0}{\mathrm{d}\theta^2}+R_mA_s\varphi_0=\frac{\mathrm{d}N_T}{\mathrm{d}\theta}, \tag{14}$$

$$\delta\varphi_0:\ (B_n-A_sR_m)\frac{\mathrm{d}u_0}{\mathrm{d}\theta}+B_n\frac{\mathrm{d}^2v_0}{\mathrm{d}\theta^2}+A_sR_mv_0+D_b\frac{\mathrm{d}^2\varphi_0}{\mathrm{d}\theta^2}-A_sR_m^2\varphi_0=\frac{\mathrm{d}M_T}{\mathrm{d}\theta}. \tag{15}$$

Boundary conditions at the edges $\theta=0$ *and* θ_0:

$$\text{Either } \delta u_0=0\quad\text{or}\quad A_s\left(\frac{\mathrm{d}u_0}{\mathrm{d}\theta}-v_0+R_m\varphi_0\right)=0, \tag{16}$$

$$\text{Either } \delta v_0=0\quad\text{or}\quad A_n\left(u_0+\frac{\mathrm{d}v_0}{\mathrm{d}\theta}\right)+B_n\frac{\mathrm{d}\varphi_0}{\mathrm{d}\theta}=N_T, \tag{17}$$

$$\text{Either } \delta\varphi_0=0\quad\text{or}\quad B_n\left(u_0+\frac{\mathrm{d}v_0}{\mathrm{d}\theta}\right)+D_b\frac{\mathrm{d}\varphi_0}{\mathrm{d}\theta}=M_T. \tag{18}$$

Free vibration equations of motion:

$$\delta u: \left(\frac{n_{0\theta\theta}+A_s}{R_m}\right)\frac{\partial^2 u}{\partial\theta^2}+\frac{1}{R_m}\left(\frac{\mathrm{d}n_{0\theta\theta}}{\mathrm{d}\theta}\right)\frac{\partial u}{\partial\theta}-\left(\frac{A_n+n_{0\theta\theta}}{R_m}\right)u-\left(\frac{A_n+A_s+2n_{0\theta\theta}}{R_m}\right)\frac{\partial v}{\partial\theta}$$
$$-\frac{1}{R_m}\left(\frac{\mathrm{d}n_{0\theta\theta}}{\mathrm{d}\theta}\right)v-\left(\frac{B_n+2\bar{N}_0}{R_m}-A_s\right)\frac{\partial\varphi}{\partial\theta}+\left(\frac{\mathrm{d}n_{0\theta\theta}}{\mathrm{d}\theta}\right)\varphi=I_{11}\frac{\partial^2 u}{\partial t^2}, \tag{19}$$

$$\delta v: \left(\frac{A_s+A_n+2n_{0\theta\theta}}{R_m}\right)\frac{\partial u}{\partial\theta}+\frac{1}{R_m}\left(\frac{\mathrm{d}n_{0\theta\theta}}{\mathrm{d}\theta}\right)u+\left(\frac{A_n+n_{0\theta\theta}}{R_m}\right)\frac{\partial^2 v}{\partial\theta^2}+\frac{1}{R_m}\left(\frac{\mathrm{d}n_{0\theta\theta}}{\mathrm{d}\theta}\right)\frac{\partial v}{\partial\theta}$$
$$-\left(\frac{A_s+n_{0\theta\theta}}{R_m}\right)v+\left(\frac{\bar{N}_0+B_n}{R_m}\right)\frac{\partial^2\varphi}{\partial\theta^2}-\left(\frac{\mathrm{d}n_{0\theta\theta}}{\mathrm{d}\theta}\right)\frac{\partial\varphi}{\partial\theta}+(A_s+n_{0\theta\theta})\varphi=I_{11}\frac{\partial^2 v}{\partial t^2}+I_{12}\frac{\partial^2\varphi}{\partial t^2}, \tag{20}$$

$$\delta\varphi: \left(\frac{B_n+2\bar{N}_0}{R_m}-A_s\right)\frac{\partial u}{\partial\theta}-\left(\frac{2Q_{0r\theta}}{R_m}+\frac{\mathrm{d}n_{0\theta\theta}}{\mathrm{d}\theta}\right)u+\left(\frac{B_n+\bar{N}_0}{R_m}\right)\frac{\partial^2 v}{\partial\theta^2}$$
$$-\left(\frac{2Q_{0r\theta}}{R_m}+\frac{\mathrm{d}n_{0\theta\theta}}{\mathrm{d}\theta}\right)\frac{\partial v}{\partial\theta}+\left(A_s-\frac{\bar{N}_0}{R_m}\right)v+\left(\frac{\bar{M}_0+D_b}{R_m}\right)\frac{\partial^2\varphi}{\partial\theta^2}+\left[2Q_{0r\theta}+R_m\left(\frac{\mathrm{d}n_{0\theta\theta}}{\mathrm{d}\theta}\right)\right]\frac{\partial\varphi}{\partial\theta}$$
$$-\left[\frac{1}{R_m}\left(\bar{M}_0-\frac{\mathrm{d}M_{0r\theta}}{\mathrm{d}\theta}\right)+R_mA_s\right]\varphi=I_{12}\frac{\partial^2 v}{\partial t^2}+I_{33}\frac{\partial^2\varphi}{\partial t^2}. \tag{21}$$

Boundary conditions at the edges $\theta=0$ *and* θ_0:

$$\text{Either } \delta u=0 \quad \text{or} \quad (A_s+n_{0\theta\theta})\left(\frac{\partial u}{\partial\theta}-v\right)-(\bar{N}_0-R_mA_s)\varphi=0, \tag{22}$$

$$\text{Either } \delta v=0 \quad \text{or} \quad (B_n+\bar{N}_0)\frac{\partial\varphi}{\partial\theta}+(A_n+n_{0\theta\theta})\left(\frac{\partial v}{\partial\theta}+u\right)+Q_{0r\theta}\varphi=0, \tag{23}$$

$$\text{Either } \delta\varphi=0 \quad \text{or} \quad (D_b+\bar{M}_0)\frac{\partial\varphi}{\partial\theta}+(B_n+\bar{N}_0)\left(\frac{\partial v}{\partial\theta}+u\right)+M_{0r\theta}\varphi=0. \tag{24}$$

In the above equations

$$N_T=\int_{R_i}^{R_o}E(r,T)\alpha(r,T)\Delta T(r)b\,\mathrm{d}r, \quad M_T=\int_{R_i}^{R_o}xE(r,T)\alpha(r,T)\Delta T(r)b\,\mathrm{d}r,$$

$$A_n=\int_{R_i}^{R_o}\left[\frac{E(r,T)}{r}\right]b\,\mathrm{d}r, \quad B_n=\int_{R_i}^{R_o}\left(\frac{x}{r}\right)E(r,T)b\,\mathrm{d}r=\int_{R_i}^{R_o}E(r,T)b\,\mathrm{d}r-R_mA_n,$$

$$A_s=\kappa\int_{R_i}^{R_o}\left[\frac{G(r,T)}{r}\right]b\,\mathrm{d}r, \quad D_b=\int_{R_i}^{R_o}E(r,T)\left(x-R_m+\frac{R_m^2}{r}\right)b\,\mathrm{d}r=\int_{R_i}^{R_o}xE(r,T)b\,\mathrm{d}r-R_mB_n,$$

$$D_s=\kappa\int_{R_i}^{R_o}\left[\frac{xG(r,T)}{r}\right]b\,\mathrm{d}r=\kappa\int_{R_i}^{R_o}G(r,T)b\,\mathrm{d}r-R_mA_s, \quad \bar{N}_0=N_{0\theta\theta}-R_mn_{0\theta\theta},$$

$$\bar{M}_0=M_{0\theta\theta}-N_{0\theta\theta}R_m+R_m^2n_{0\theta\theta}. \tag{25}$$

Also, the resultant forces and moments are related to the displacement components, the bending rotation and the temperature rise as

$$\begin{Bmatrix}N_{0\theta\theta}\\ n_{0\theta\theta}\\ M_{0\theta\theta}\end{Bmatrix}=\begin{bmatrix}A_n & B_n\\ a_n & b_n\\ B_n & D_b\end{bmatrix}\begin{Bmatrix}\frac{\partial v_0}{\partial\theta}+u_0\\ \frac{\partial\varphi_0}{\partial\theta}\end{Bmatrix}-\begin{Bmatrix}N_T\\ n_T\\ M_T\end{Bmatrix}, \quad \begin{Bmatrix}Q_{0r\theta}\\ M_{0r\theta}\end{Bmatrix}=\begin{Bmatrix}A_s\\ D_s\end{Bmatrix}\left(\frac{\partial u_0}{\partial\theta}-v_0+R_m\varphi_0\right) \tag{26}$$

with

$$n_T = \int_{R_i}^{R_o} E(r,T)\alpha(r,T)\left(\frac{\Delta T(r)}{r}\right) b\,\mathrm{d}r, \quad a_n = \int_{R_i}^{R_o}\left[\frac{E(r,T)}{r^2}\right] b\,\mathrm{d}r, \quad b_n = A_n - R_m a_n.$$

Different types of the classical boundary conditions at the edges $\theta = 0$ and θ_0 of the arch can be obtained by combining the conditions stated in Eqs. (16)–(18) for the thermoelastic equilibrium analysis and Eqs. (22)–(24) for the free vibration analysis. For example, for the equilibrium state one has

$$\text{Simply supported (S)}: \quad u_0 = 0, \quad v_0 = 0, \quad B_n\left(u_0 + \frac{\mathrm{d}v_0}{\mathrm{d}\theta}\right) + D_b\frac{\mathrm{d}\varphi_0}{\mathrm{d}\theta} = M_T, \tag{27}$$

$$\text{Clamped (C)}: \quad u_0 = 0, \quad v_0 = 0, \quad \varphi_0 = 0, \tag{28}$$

$$\text{Free (F)}: \quad \frac{\mathrm{d}u_0}{\mathrm{d}\theta} - v_0 + R_m\varphi_0 = 0, \quad A_n\left(u_0 + \frac{\mathrm{d}v_0}{\mathrm{d}\theta}\right) + B_n\varphi_0 = N_T,$$

$$B_n\left(u_0 + \frac{\mathrm{d}v_0}{\mathrm{d}\theta}\right) + D_b\frac{\mathrm{d}\varphi_0}{\mathrm{d}\theta} = M_T. \tag{29}$$

3. Solution procedure

Analytical solutions to the above system of equations cannot be found, thus, here DQM as an approximate but efficient numerical tool is employed to solve these equations. Details of this procedure can be found in the previous works of Malekzadeh and his co-workers [5,16–18,22]. However, for the purpose of completeness, a brief review of the DQM is presented here.

The basic idea of the differential quadrature method is that the derivative of a function with respect to a coordinate variable at a given grid point is approximated as the linear weighted sums of its values at all of the grid points in the domain of that variable. In order to illustrate the DQ approximation, consider a function $f(\theta,t)$ having its field on a domain $0 \le \theta \le \theta_0$, $0 \le t$. Based on the DQM, the domain is discretized into N_θ grid points along the θ-direction. Then, at each grid point (θ_i) with $i = 1,2,3,\ldots,N_\theta$, the first- and second-order partial derivatives of the function $f(\theta,t)$ with respect to θ are approximated as

$$\left.\frac{\partial f(\theta,t)}{\partial\theta}\right|_{\theta=\theta_i} = \sum_{m=1}^{N_\theta} A_{im}^{\theta} f(\theta_m,t) = \sum_{m=1}^{N_\theta} A_{im}^{\theta} f_m(t), \quad \left.\frac{\partial^2 f(\theta,t)}{\partial\theta^2}\right|_{\theta=\theta_i} = \sum_{m=1}^{N_\theta} B_{im}^{\theta} f_m(t), \tag{30}$$

where A_{ij}^{θ} and B_{ij}^{θ} are the DQ weighting coefficient of the first- and second-order derivatives. From this equation one can deduce that the important components of DQ approximations are the weighting coefficients and the choice of sampling points. In order to determine the weighting coefficients, a set of test functions should be used in Eq. (30). For polynomial basis functions DQ, a set of Lagrange polynomials are employed as the test functions. The weighting coefficients for the first-order derivatives in the θ-direction are thus determined as [15]

$$A_{ij}^{\theta} = \begin{cases} \dfrac{1}{\theta_0(\theta_i-\theta_j)}\dfrac{\prod_{k=1,i\neq k}^{N_\theta}(\theta_i-\theta_k)}{\prod_{k=1,j\neq k}^{N_\theta}(\theta_j-\theta_k)} & \text{if } i\neq j \\ -\sum\limits_{\substack{k=1\\ i\neq j}}^{N_\theta} A_{ik}^{\theta} & \text{if } i=j \end{cases} \quad \text{for } i,j = 1,2,\ldots,N_\theta. \tag{31}$$

Using the weighting coefficients of the first-order derivative, the weighting coefficients of the second-order derivative are obtained as [15]

$$\mathbf{B^{\theta}} = \mathbf{A^{\theta}A^{\theta}} = (\mathbf{A^{\theta}})^2. \tag{32}$$

A natural grid generation rule is that of equally spaced points. However, a better choice is that corresponding to zeros of the orthogonal polynomials such as the zeros of the Chebyshev polynomials or the so-called cosine-type grid generation rule. In this study, this type of grid generation rule is used [15]

$$\frac{\theta_i}{\theta_0} = \frac{1}{2}\left\{1 - \cos\left[\frac{(i-1)\pi}{(N_\theta-1)}\right]\right\} \quad \text{for } i = 1,2,3,\ldots,N_\theta. \tag{33}$$

Employing the DQ rules to the thermoelastic equilibrium equations at each domain grid point θ_i with $i=2,3,\ldots,N_\theta-1$ and at the boundary grid points $\theta_1=0$ and $\theta_{N_\theta}=\theta_0$ to discretize the related boundary conditions, one obtains a system of algebraic equations which in the matrix form become [16]

$$\mathbf{S}\mathbf{U}_0=\mathbf{F}, \tag{34}$$

where $\mathbf{U}_0$ is the vector of unknown degrees of freedom

$$\mathbf{U}_0=[u_{01}\ \ \ldots\ \ u_{0N_\theta}\ \ v_{01}\ \ \ldots\ \ v_{0N_\theta}\ \ \varphi_{01}\ \ \ldots\ \ \varphi_{0N_\theta}]^{\mathrm{T}}. \tag{35}$$

Hereafter, $f_i=f(\theta_i)$. $\mathbf{S}$ is the stiffness matrix and its elements are obtained from the discretized differential equations and boundary conditions based on the definition (35) and $\mathbf{F}$ the load vector. After solving this system of algebraic equations, the displacement components at the DQ grid points are obtained. Then, the initial thermal resultant forces and moments at each DQ grid points θ_i are obtained from the constitutive relations (26) as

$$\begin{Bmatrix}(N_{0\theta\theta})_i\\(n_{0\theta\theta})_i\\(M_{0\theta\theta})_i\end{Bmatrix}=\begin{bmatrix}A_n & B_n\\ a_n & b_n\\ B_n & D_b\end{bmatrix}\begin{Bmatrix}\sum_{m=1}^{N_\theta}A_{im}^{\theta}v_{0m}+u_{0i}\\ \sum_{m=1}^{N_\theta}A_{im}^{\theta}\varphi_{0m}\end{Bmatrix}-\begin{Bmatrix}(N_T)_i\\(n_T)_i\\(M_T)_i\end{Bmatrix},$$

$$\begin{Bmatrix}(Q_{0r\theta})_i\\(M_{0r\theta})_i\end{Bmatrix}=\begin{Bmatrix}A_s\\D_s\end{Bmatrix}\left(\sum_{m=1}^{N_\theta}A_{im}^{\theta}u_{0m}-v_{0i}+R_m\varphi_{0i}\right)\quad\text{for } i=1,2,\ldots,N_\theta, \tag{36}$$

where $()_i=()|_{\theta=\theta_i}$.

At this stage the DQ rules are employed to discretize the free vibration equations and the related boundary conditions. In order to carry out the eigenvalue analysis, the domain and boundary degrees of freedom should be separated. In vector forms, they are denoted as $\{d\}$, and $\{b\}$, respectively. Based on these definitions and using Eq. (36), the DQ discretized form of the equations of motion and the related boundary conditions can be obtained in the matrix form as [5,22]

Equations of motion:

$$\mathbf{S_{db}}\mathbf{b}+\mathbf{S_{dd}}\mathbf{d}+\mathbf{M}\ddot{\mathbf{d}}=\mathbf{0}. \tag{37}$$

Boundary conditions:

$$\mathbf{S_{bb}}\mathbf{b}+\mathbf{S_{bd}}\mathbf{d}=\mathbf{0}. \tag{38}$$

The elements of the stiffness matrixes $\mathbf{S_{di}}$ $(i=b,d)$ and the mass matrix $\mathbf{M}$ are obtained from equations of motion and those of the stiffness matrixes $\mathbf{S_{bi}}$ $(i=b,d)$ are obtained from the boundary conditions.

Eliminating the boundary degrees of freedom from Eq. (37) using Eq. (38) and considering $\mathbf{d}(t)=\mathbf{D}\,\mathrm{e}^{\mathrm{I}\omega t}$, in which ω is the natural frequency and $\mathrm{I}(=\sqrt{-1})$ is the imaginary number, the result reads

$$(\bar{\mathbf{S}}-\omega^2\mathbf{M})\mathbf{D}=0, \tag{39}$$

where $\bar{\mathbf{S}}=\mathbf{S_{dd}}-\mathbf{S_{db}}\mathbf{S_{bb}^{-1}}\mathbf{S_{bd}}$.

Solving the eigenvalue system of Eq. (39), the natural frequencies and mode shapes of the arches will be obtained.

Table 1
Temperature-dependent coefficients of material properties for ceramic (ZrO_2) and metals (Ti–6Al–4 V) [20].

	Material	Q_0	Q_1	Q_2
E	Ti–6Al–4V	122.7 (GPa)	-4.605×10^{-4}	0
	ZrO_2	132.2 (GPa)	-3.805×10^{-4}	-6.127×10^{-8}
v	Ti–6Al–4V	0.2888	1.108×10^{-4}	0
	ZrO_2	0.3330	0	0
ρ	Ti–6Al–4V	4420 (kg/m^3)	0	0
	ZrO_2	3657 (kg/m^3)	0	0
α	Ti–6Al–4V	7.43×10^{-6} (1/K)	7.483×10^{-4}	-3.621×10^{-7}
	ZrO_2	13.3×10^{-6} (1/K)	-1.421×10^{-3}	9.549×10^{-7}
K	Ti–6Al–4V	6.10 (W/m K)	0	0
	ZrO_2	1.78 (W/m K)	0	0

Table 2
Convergence of the first three non-dimensional natural frequency parameters of clamped FG arch under uniform temperature rise ($p=2$, $\Delta T=800$ K).

θ_0	N_θ	$h/R_m=0.1$			$h/R_m=0.2$		
		λ_1	λ_2	λ_3	λ_1	λ_2	λ_3
60°	7	21.642	30.877	60.812	13.860	23.073	35.489
	9	21.630	29.733	57.285	13.862	22.829	35.287
	13	21.630	29.731	57.263	13.862	22.827	35.283
	17	21.630	29.731	57.263	13.862	22.827	35.283
	19	21.630	29.731	57.263	13.862	22.827	35.283
120°	7	7.7572	14.915	24.520	6.8323	8.9184	16.298
	9	7.3280	13.196	22.136	6.6033	8.7945	14.920
	13	7.3284	13.132	21.931	6.6032	8.7922	14.878
	17	7.3285	13.132	21.931	6.6032	8.7922	14.878
	19	7.3285	13.132	21.931	6.6032	8.7922	14.878

Table 3
Convergence of the first three non-dimensional natural frequency parameters of clamped FG arch under non-uniform (nonlinear) temperature rise ($p=2$, $\Delta T_m=0$, $\Delta T_c=800$ K).

θ_0	N_θ	$h/R_m=0.1$			$h/R_m=0.2$		
		λ_1	λ_2	λ_3	λ_1	λ_2	λ_3
60°	7	26.163	37.273	73.075	16.788	28.060	42.169
	9	26.151	35.931	68.930	16.791	27.762	41.955
	13	26.150	35.929	68.907	16.791	27.760	41.950
	17	26.150	35.929	68.907	16.791	27.760	41.950
	19	26.150	35.929	68.907	16.791	27.760	41.950
120°	7	9.2294	17.871	29.368	8.1980	10.755	19.576
	9	8.7122	15.756	26.533	7.9217	10.604	17.922
	13	8.7127	15.676	26.284	7.9216	10.601	17.871
	17	8.7127	15.676	26.284	7.9216	10.601	17.871
	19	8.7127	15.676	26.284	7.9216	10.601	17.871

Table 4
Comparison of the first three non-dimensional natural frequency parameters of the isotropic arch ($v=0.3$).

	θ_0	$h/R_m=0.1$			$h/R_m=0.2$		
		λ_1	λ_2	λ_3	λ_1	λ_2	λ_3
C–C	60°	33.981	47.025	89.869	21.782	35.946	54.374
FSDST [1]		33.981	47.021	89.863	21.777	35.911	54.299
2D-LW-DQ [5]		34.041	47.259	90.462	21.910	36.368	54.594
S–S		31.569	31.734	71.449	17.068	27.671	53.900
FSDST [1]		31.569	31.732	71.446	17.067	27.655	53.822
C–S		31.595	39.735	80.686	18.816	32.186	53.985
FSDST [1]		31.594	39.732	80.682	18.814	32.161	53.909
C–C	120°	11.392	20.393	34.001	10.279	13.665	23.116
FSDST [1]		11.391	20.392	34.001	10.271	13.662	23.107
2D-LW-DQ [5]		11.411	20.436	34.044	10.333	13.718	23.254
S–S		6.8254	16.586	31.731	6.5488	13.461	18.978
FSDST [1]		6.8247	16.585	31.730	6.5450	13.458	18.975
C–S		8.9605	18.664	32.768	8.3067	13.613	20.934
FSDST [1]		8.9595	18.663	32.767	8.3012	13.610	20.928

4. Numerical results

In this section, firstly, the convergence and accuracy of the method is investigated and then the effects of the geometrical and the material parameters on the in-plane free vibration characteristics of FG circular arches under uniform ($\Delta T_c=\Delta T_m=\Delta T$) and non-uniform temperature rise ($\Delta T_m=0$, $\Delta T_c=\Delta T$) are presented. In the examples solved, unless

Table 5

Convergence and accuracy of the fundamental non-dimensional natural frequency parameter $\left[\sqrt[4]{(\rho_0 A_0 L^4 \omega^2)/(E_0 I_{xx})}\right]$[a] of the soft simply supported FG straight beam [$b/h = 1$, $g = \ln(10)$, $L(= R_m\theta_0) = R_m = 1$, $\nu = 0.3$].

H/L	N_θ					2D-analytic [11]
	7	9	13	19	23	
1/15	2.9459	2.9453	2.9454	2.9454	2.9454	2.9449
1/5	2.8837	2.8832	2.8832	2.8832	2.8832	2.8773

[a] E_0 and ρ_0 are the Young's modulus and the mass density of ceramic [11]; $I_{xx} = bh^3/12$, $A_0 = bh$.

otherwise specified, the following non-dimensional frequency parameter is used

$$\lambda_i = \omega_i (R_m^2/h)\sqrt{\rho_{0c}/E_{0c}}. \tag{40}$$

The material properties of Ti–6Al–4V and ZrO_2, as given in Table 1, are used in the numerical computations. They are valid for the temperature range of $300 \le T \le 1100$ K [20,21].

4.1. Convergence study and validation

Lack of appropriate results for functionally graded circular arches for direct comparison has forced us to validate the presented formulation in one of the two following ways. First, compare the results with those of isotropic arches and second, observe the convergence of the solutions with respect to increasing N_θ, the number of discrete points distributed along the θ-directions.

As a first example to validate the presented formulations, the convergence of the method for FG arches with temperature-dependent material properties under high temperature thermal environment is studied here. The results for the FG clamped arches under high uniform temperature rise are presented in Table 2 and those of the FG clamped arches subjected to non-uniform temperature rise are presented in Table 3. In all cases, fast rate of convergence of the method are evident. It should be mentioned that for both uniform and non-uniform temperature rise, only nine DQ grid points in the tangential direction is sufficient to obtain results with sufficient accuracy. Also, in all cases for $N_\theta \ge 13$ the results will find no change up to five significant digits. Hence, hereafter, the results for the FG arches are prepared using $N_\theta = 13$.

As another attempt to validate the presented formulations, in Table 4 the first three non-dimensional natural frequency parameters of the isotropic arches subjected to different boundary conditions are compared with those obtained using the Qatu's formulation [1], which are based on the first-order shear deformation shell theory (FSDST). The results are prepared for two different values of the opening angle (θ_0) and the thickness-to-length ratio. Additionally, the same problem but with clamped boundary conditions is also solved by using the two-dimensional layerwise-differential quadrature (2D-LW-DQ) method presented by Malekzadeh et al. [5], which its high accuracy was demonstrated. The converged results of the 2D-LW-DQ are obtained by using 12 mathematical layers in the radial direction and 70 grid points in the tangential direction. In all cases, excellent agreements with those of the other two approaches have been achieved.

Also to verify the accuracy of the method for FG beams, the solutions for the fundamental frequency parameter of a soft simply supported straight beam are compared with those of two-dimensional analytical elasticity solution of Ying et al. [11] in Table 5. They assumed that all elastic constants and mass density varied exponentially through the beam thickness, that is $\overline{Q} = \overline{Q}_0\, e^{gz}$, where $\bar{Q}$ represents elastic constant or mass density of the beam, g the gradient index and z the through thickness coordinate ($z = r - R_i$, in the present analysis). The numerical values of the material properties are the same as those given in Ref. [11]. From the data presented in Table 5, which are prepared for two different values of the thickness-to-length ratios, the fast rate of convergence and high accuracy of the method are evident.

4.2. Parametric studies

In this section, unless otherwise stated, the following value are used for the chosen parameter in the examples considered; $p = 2$, $\theta_0 = 120^\circ$, $h = 0.2R_m$. To show the importance of considering the variation of material properties with temperature, the first two frequency parameters of the FG circular arches with and without the temperature-dependent material properties subjected to non-uniform temperature rise are compared in Figs. 2(a)–(c). The results are prepared for FG arches with three different sets of boundary conditions at edges: clamped–clamped, clamped–simply supported and simply supported–simply supported. From these figures one can see that the frequency parameters are greatly overestimated when the temperature-dependence of material parameters is not taken into account. The discrepancy between temperature-dependent and temperature-independent solutions increase dramatically as the temperature rise increases. The relative errors between the results of the two formulations at $\Delta T = 800$ K are presented in Table 6. The difference reaches as high as 20.772 percent for the second frequency parameters of simply supported arch.

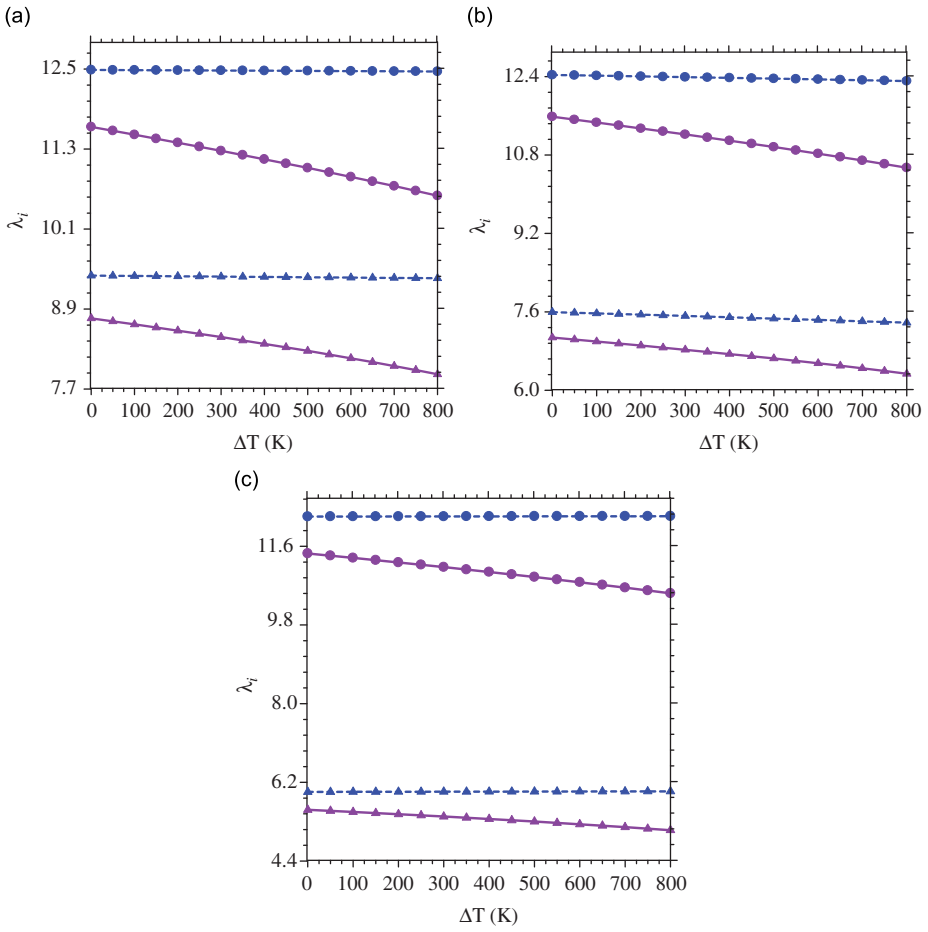

Fig. 2. (a)–(c). Comparison of the first two frequency parameters of the (a) clamped, (b) simply support–clamped and (c) simply supported FG circular arches with and without the temperature-dependent material properties. Temperature dependent: the first mode ($i = 1$), the second mode ($i = 2$); Temperature independent: the first mode ($i = 1$), the second mode ($i = 2$).

Table 6
Relative error[a] between the results for the FG arch with and without the temperature-dependent properties at $\Delta T = 800$ K.

Boundary conditions	e_1	e_2	e_3
Clamped	18.177	17.573	18.033
Simply supported–clamped	16.455	16.784	18.142
Simply supported	17.401	16.757	20.772

[a] $e_i = [(\lambda_i)_{\text{Temperature-dependent}} - (\lambda_i)_{\text{Temperature-independent}}] \times 100/(\lambda_i)_{\text{Temperature-dependent}}$.

In some studies in free vibration analysis of FG plates, pre-stress analysis has not been used and usually the initial thermal stresses have been obtained approximately from the thermal strains; see for example Refs. [20,23]. For the circular arch these approximate formulations reduce to

$$\sigma_{0\theta\theta} = -E(r,T)\alpha(r,T)\Delta T, \quad \sigma_{0r\theta} = 0. \tag{41}$$

In Figs. 3(a)–(c), a comparison between the obtained results based on using Eqs. (10) and (41) for the initial thermal stresses are made. The first three frequency parameters of simply supported FG circular arches under non-uniform temperature rise are presented. It is interesting to note that the effect of approximate evaluation of the initial stresses on the fundamental frequency parameters is more than the other two frequency parameters (see also Table 7). The difference between the results of the two approaches increases by increasing the temperature rise. The natural frequencies obtained

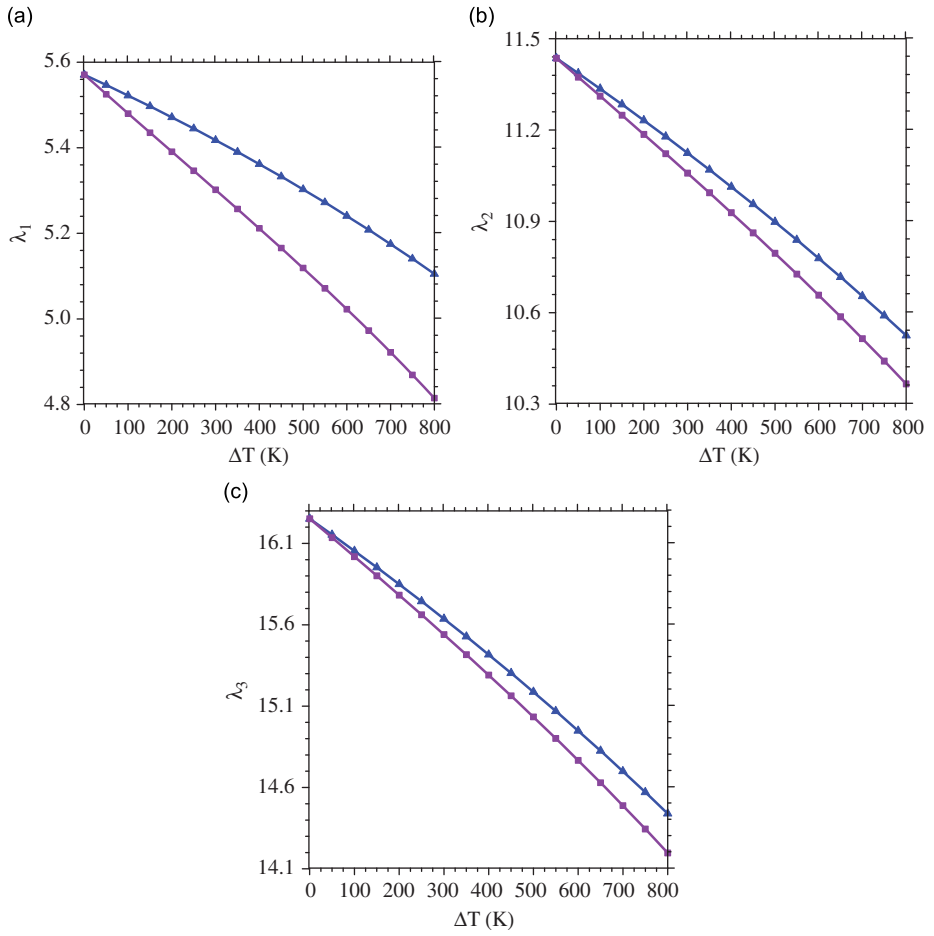

Fig. 3. (a)–(c). The effects of approximate evaluation of the thermal stresses on the first three frequency parameters of simply supported FG arches: without approximation and with approximation.

Table 7
Relative error[a] between the results for the FG arch with and without approximate evaluation of thermal stresses at $\Delta T = 800\,\mathrm{K}$.

Boundary conditions	e_1	e_2	e_3
Clamped	2.2610	1.0318	1.1674
Simply supported–clamped	2.3632	0.7612	0.6030
Simply supported	6.0274	1.5344	1.7028

[a] $e_i = [(\lambda_i)_{\text{Without app.}} - (\lambda_i)_{\text{With app.}}] \times 100/(\lambda_i)_{\text{Without app.}}$.

based the approximate theory is lower than those of the exact formulation because the initial thermal stresses obtained using the approximate theory are higher than those obtained by exact formulation.

The effects of uniform and non-uniform temperature rise on the first three frequency parameters of clamped FG arches are shown in Figs. 4(a)–(c). It can be seen that for identical change of temperature rise, the uniform temperature rise has more effect than non-uniform temperature rise on the frequency parameters and increasing the temperature rise, the discrepancy between the results of the two cases increase dramatically. This is because for the same value of the uniform temperature rise, the variation of the material properties and also the value of the thermal stresses are greater than those of non-uniform one.

The influences of the opening angle (θ_0) on the first three frequency parameters of FG clamped circular arches under non-uniform temperature rise are presented in Figs. 5(a) and (b) for two different values of thickness-to-mean radius ratio. It can be seen that increasing the opening angle, the frequency parameters decrease. This is due to the fact that increasing the opening angle, the beam length increases and consequently the stiffness reduces.

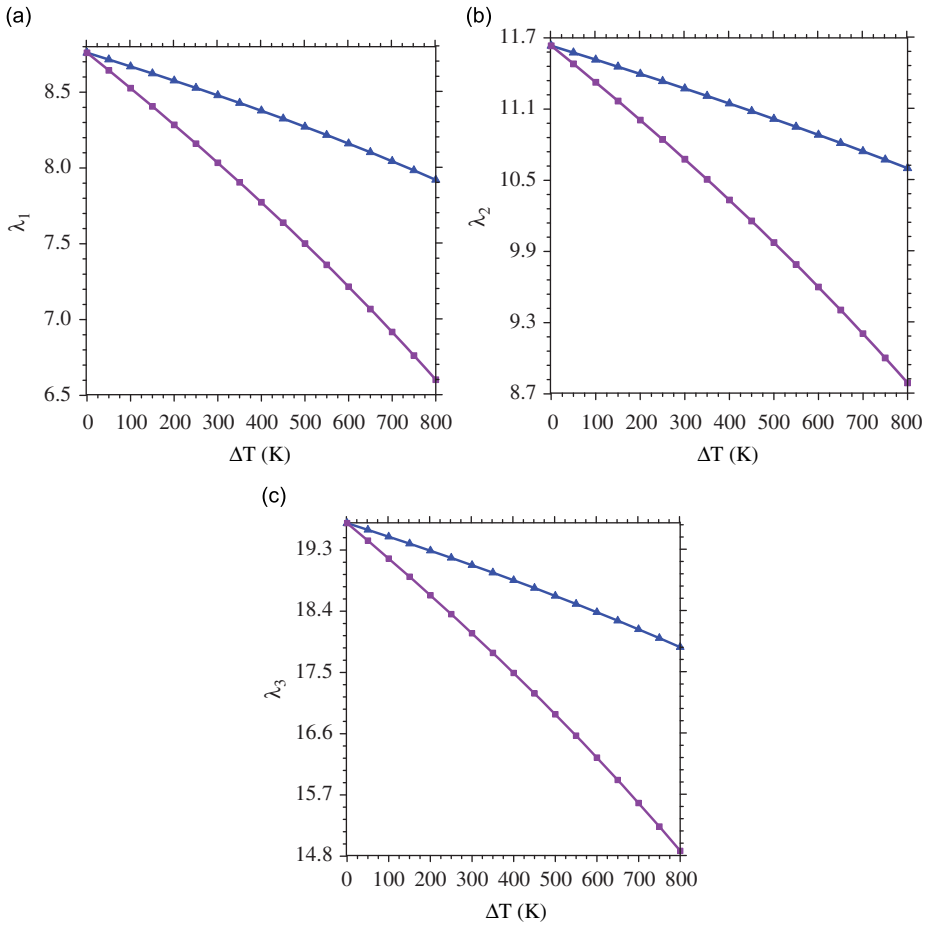

Fig. 4. (a)–(c). The effects of the uniform and non-uniform temperature rise on the first three frequency parameters of the clamped FG arches: non-uniform and uniform.

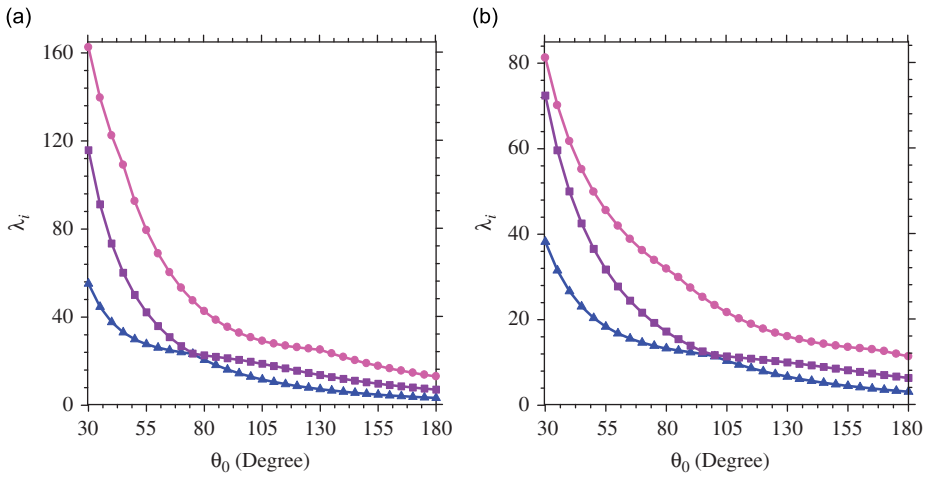

Fig. 5. (a, b). The effects of the opening angle (θ_0) on the first three frequency parameters of the clamped FG arches: (a) $h/R_m = 0.1$ and (b) $h/R_m = 0.2$; the first mode ($i = 1$), the second mode ($i = 2$), the third mode ($i = 3$).

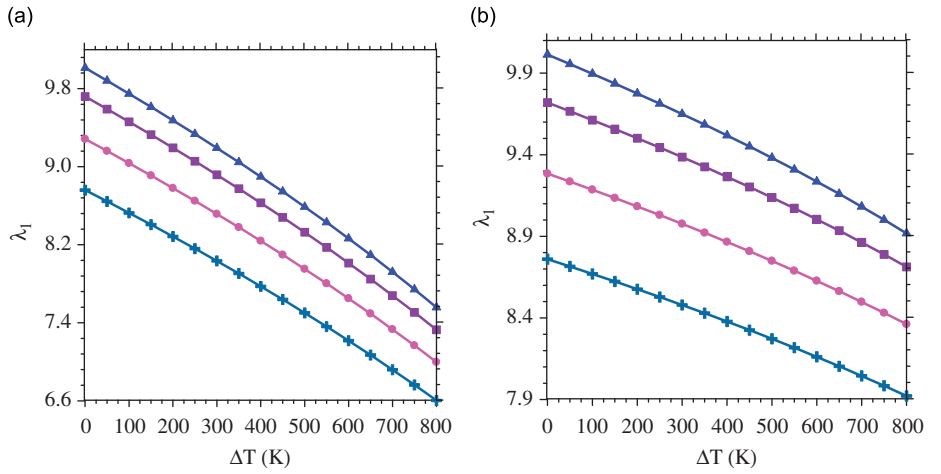

Fig. 6. (a, b). The effects of the thickness-to-mean radius ratio (h/R_m) on the fundamental frequency parameter of the clamped FG arches subjected to the (a) uniform temperature rise and (b) non-uniform temperature rise: $h/R_m = 0.05$, $h/R_m = 0.1$, $h/R_m = 0.15$ and $h/R_m = 0.2$.

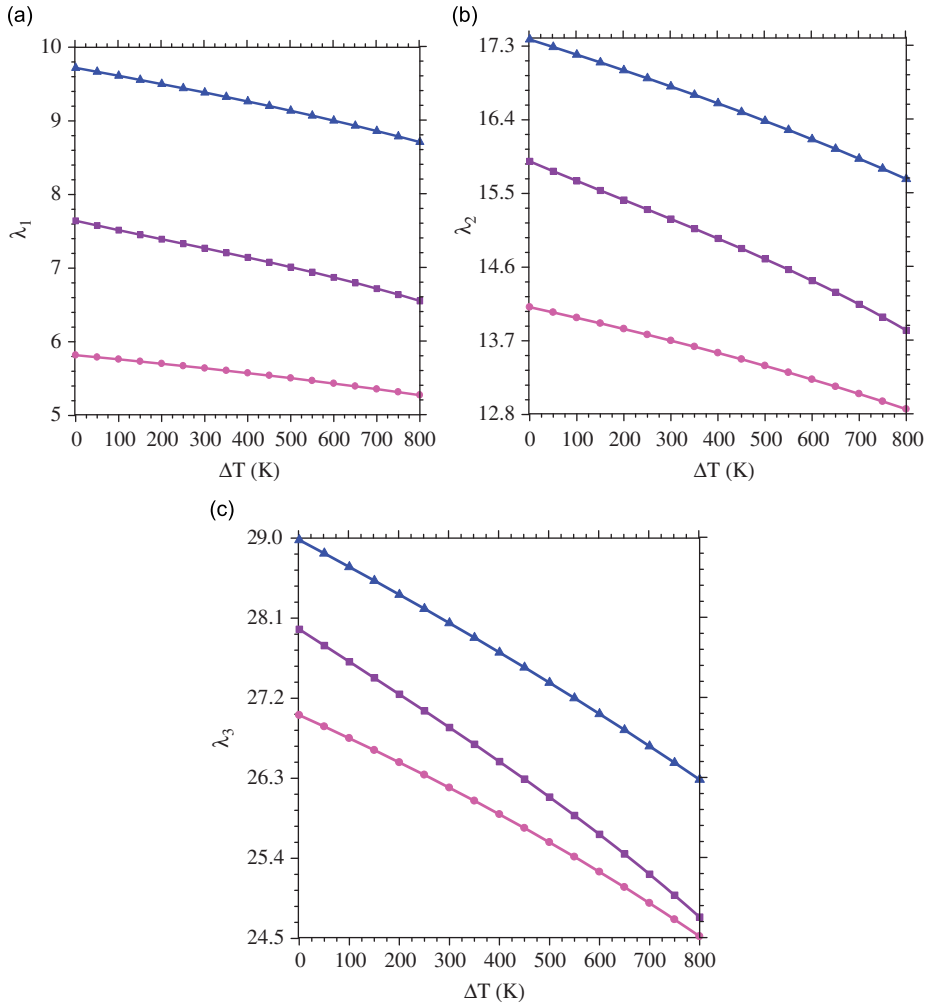

Fig. 7. (a)–(c). Comparison of the first three frequency parameters of the FG arches with three different boundary conditions subjected to the non-uniform temperature rise ($h = 0.1R_m$): C–C, C–S and S–S.

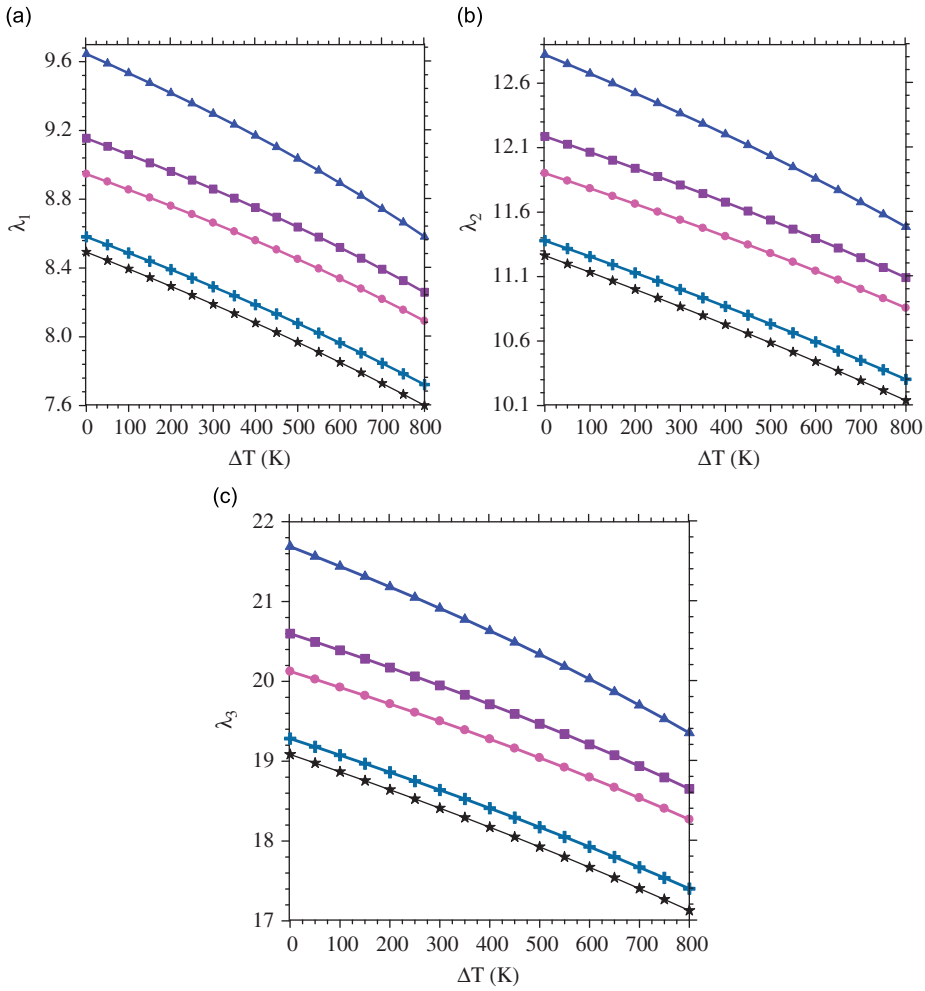

Fig. 8. (a)–(c). The effects of the material index parameter (p) on the first three frequency parameters of the clamped FG arches subjected to the non-uniform temperature rise: $p = 0$, $p = 0.5$, $p = 1$, $p = 5$ and $p = 10$.

The results for the fundamental frequency parameter of the FG clamped circular arches for different values of thickness-to-mean radius ratio and under uniform and non-uniform temperature rise are compared in Figs. 6(a) and (b). Presented in Figs. 7(a)–(c) are comparison between the results for the first three frequency parameters of the FG arches with three different sets of boundary conditions and subjected to non-uniform temperature rise. As it can be seen, in all cases, increasing the temperature rise, due to reduction in the elastic coefficients the natural frequencies decrease.

The effects of the material index (p) on the first three frequency parameters of FG clamped circular arches subjected to non-uniform temperature rise are presented in Fig. 8. It can be seen that increasing the material index (p), the frequency parameters decrease. Through the numerical experiment, the same behavior is observed for FG arches with other types of boundary conditions.

5. Conclusion

A method for the in-plane free vibration analysis of the FG circular arches with temperature-dependent material properties subjected to thermal environment was presented. Employing the Hamilton's principle, the equations of motion and the related boundary conditions subjected to initial thermal stresses were derived. The initial thermal stresses were obtained by solving the thermoelastic equilibrium equations of the arch. DQM as an efficient numerical tool is used to solve the system of equations. The methodology has the capacity to provide solutions for arches with different types of boundary conditions. The effects of the temperature rise, boundary conditions and the material graded index as well as the different geometrical parameters such as the thickness-to-mean radius ratio and the opening angle on the frequency parameters of the FG arches were investigated. It was shown that the temperature-dependence material properties can have significant impacts on the natural frequencies.

References

[1] M.S. Qatu, Theories and analysis of thin and moderately thick laminated composite curved beams, *International Journal of Solids and Structures* 30 (1993) 2743–2756.
[2] V. Yildirim, Rotary inertia, axial and shear deformation effects on the in-plane natural frequencies of symmetric cross-ply laminated circular arches, *Journal of Sound and Vibration* 224 (1999) 575–589.
[3] Y.P. Tseng, C.S. Huang, M.S. Kao, In-plane vibration of laminated curved beams with variable curvature by dynamic stiffness analysis, *Composite Structures* 50 (2000) 103–114.
[4] H. Matsunaga, Free vibration and stability of laminated composite circular arches subjected to initial axial stress, *Journal of Sound and Vibration* 271 (2004) 651–670.
[5] P. Malekzadeh, A.R. Setoodeh, E. Barmshouri, A hybrid layerwise and differential quadrature method for in-plane free vibration of laminated thick circular arches, *Journal of Sound and Vibration* 315 (2008) 212–225.
[6] Q. Lü, C.F. Lü, Exact two-dimensional solutions for in-plane natural frequencies of laminated circular arches, *Journal of Sound and Vibration* 318 (2008) 982–990.
[7] M. Aydogdu, V. Taskin, Free vibration analysis of functionally graded beams with simply supported edges, *Materials and Design* 28 (2007) 1651–1656.
[8] X.-F. Li, A unified approach for analyzing static and dynamic behaviors of functionally graded Timoshenko and Euler–Bernoulli beams, *Journal of Sound and Vibration* 318 (2008) 1210–1229.
[9] S.A. Sina, H.M. Navazi, H. Haddadpour, An analytical method for free vibration analysis of functionally graded beams, *Materials and Design* 30 (2009) 741–747.
[10] J. Yang, Y. Chen, Free vibration and buckling analyses of functionally graded beams with edge cracks, *Composite Structures* 83 (2008) 48–60.
[11] J. Ying, C.F. Lü, W.Q. Chen, Two-dimensional elasticity solutions for functionally graded beams resting on elastic foundations, *Composite Structures* 84 (2008) 209–219.
[12] R.K. Bhangale, N. Ganesan, Thermoelastic buckling and vibration behavior of a functionally graded sandwich beam with constrained viscoelastic core, *Journal of Sound and Vibration* 295 (2006) 294–316.
[13] S.C. Pradhan, T. Murmu, Thermo-mechanical vibration of FGM sandwich beam under variable elastic foundations using differential quadrature method, *Journal of Sound and Vibration* 321 (2009) 342–362.
[14] H.J. Xiang, J. Yang, Free and forced vibration of a laminated FGM Timoshenko beam of variable thickness under heat conduction, *Composites Part B: Engineering* 39 (2008) 292–303.
[15] C.W. Bert, M. Malik, Differential quadrature method in computational mechanics: a review, *Applied Mechanics Reviews* 49 (1996) 1–27.
[16] P. Malekzadeh, G. Karami, Out-of-plane static analysis of circular arches by DQM, *International Journal of Solids and Structures* 40 (2003) 6527–6545.
[17] G. Karami, P. Malekzadeh, In-plane free vibration analysis of circular arches with varying cross sections, *Journal of Sound and Vibration* 274 (2004) 777–799.
[18] S.A. Fazelzadeh, P. Malekzadeh, P. Zahedinejad, M. Hosseini, Vibration analysis of functionally graded thin-walled rotating blades under high temperature supersonic flow using the differential quadrature method, *Journal of Sound and Vibration* 306 (2007) 333–348.
[19] L. Yang, S. Zhifei, Free vibration of a functionally graded piezoelectric beam via state-space based differential quadrature, *Composite Structures* 87 (2009) 257–264.
[20] Y.W. Kim, Temperature dependent vibration analysis of functionally graded rectangular plates, *Journal of Sound and Vibration* 284 (2005) 531–549.
[21] Y.S. Touloukian, *Thermophysical Properties of High Temperature Solid Materials*, MacMillan, New York, 1967.
[22] T. Prakash, M. Ganapathi, Asymmetric flexural vibration and thermoelastic stability of FGM circular plates using finite element method, *Composites Part B: Engineering* 37 (2006) 642–649.
[23] P. Malekzadeh, Three-dimensional free vibration analysis of thick functionally graded plates on elastic foundations, *Composite Structures* 89 (2009) 367–373.